Supporting Information

Mani et al. 10.1073/pnas.1307459110

SI Text

1. Diffusive Propagation of Signals

As stated in the main text, the stoichiometric constraint ensures the propagation of polarization. We show here that in the limit of linear heterodimer kinetics, the propagation is effectively diffusive with a length scale $\xi = \sqrt{\frac{k_u \gamma_u^{-1}(d^0+f^0)}{2}}$, where d^0 and f^0 are the uniform concentrations of total cellular Dachsous (Ds) and Fat.

Restricting ourselves to one dimension:

$$k_u^{-1}\frac{dU_{i,i+1}}{dt} = -\left(k_u^{-1}\gamma_u + d^0_{i+1} + f^0_i\right)U_{i,i+1} - d^0_{i+1}U_{i,i-1} - f^0_i U_{i+2,i+1} + f^0_i d^0_{i+1} + \left(U_{i,i+1}+U_{i,i-1}\right)\left(U_{i,i+1}+U_{i-2,i+1}\right)$$

$$k_u^{-1}\frac{dU_{i+1,i}}{dt} = -\left(k_u^{-1}\gamma_u + d^0_i + f^0_{i+1}\right)U_{i+1,i} - d^0_i U_{i+1,i+2} - f^0_i U_{i-1,i} + f^0_{i+1} d^0_i + \left(U_{i+1,i}+U_{i+1,i+2}\right)\left(U_{i+1,i}+U_{i+1,i-1}\right).$$

Linearizing, assuming close to uniform Fat and Ds (which allows us to drop their subscripts), and focusing on the dipole moment gives

$$k_u^{-1}\frac{dq_{i,i+1}}{dt} = -\left[k_u^{-1}\gamma_u + d^0 + f^0\right]q_{i,i+1} + \frac{1}{2}\left(d^0+f^0\right)\left(q_{i-1,i}+q_{i+1,i+2}\right) + I_{i,i+1}$$

$$= -k_u^{-1}\gamma_u q_{i,i+1} + \frac{1}{2}\left(d^0+f^0\right)\nabla^2 q_{i,i+1} + I_{i,i+1},$$

where ∇^2 denotes the 1D-lattice Laplacian. This is recognized as a damped diffusion equation for the dipole moment $q_{i,i+1}$ with a "source term":

$$I_{i,i+1} = \left(f^0_i d^0_{i+1} - f^0_{i+1} d^0_i\right) - \frac{1}{2}\left(d^0+f^0\right) \times \left(U_{i,i-1}+U_{i-1,i}+U_{i+2,i+1}+U_{i+1,i+2}\right).$$

From this equation, we can read off the characteristic diffusive length scale given by a square root of the ratio of the diffusivity to damping:

$$\xi = \sqrt{\frac{k_u \gamma_u^{-1}\left(d^0+f^0\right)}{2}}. \quad \text{[S1]}$$

2. Level and Gradient Dependence of Alternative Interaction Models

We explore the steady-state heterodimer concentration as a function of protocadherin level and gradient. To simplify the analysis, we hold one protocadherin level, say Fat, constant at $f^0_i = f^0$. For a slowly varying Ds profile [parameterized locally by $d^0_i/f^0 = D$ and $\Delta D = (d^0_{i+1} - d^0_i)/f^0$, with $\Delta D \ll D$], the steady state is described by the following coupled algebraic equations:

$$(1-s)(D+\Delta D - s)\left(1+\alpha\left[\frac{s+q}{2}\right]\right) - \Gamma\left[\frac{s+q}{2}\right]\left(1+\beta\left[\frac{s-q}{2}\right]\right) = 0 \quad \text{[S2]}$$

$$(1-s)(D-\Delta D - s)\left(1+\alpha\left[\frac{s-q}{2}\right]\right) - \Gamma\left[\frac{s-q}{2}\right]\left(1+\beta\left[\frac{s+q}{2}\right]\right) = 0, \quad \text{[S3]}$$

where local heterodimer abundances have been expressed in terms of dimensionless s and q. $\Gamma = \frac{\gamma_u}{k_u f^0}$ is the dimensionless degradation constant. α and β have also been appropriately scaled by f^0.

i) $\alpha = 0$ and $\beta = 0$:

$$2(1-s)(D-s) - \Gamma s = 0 \quad \text{[S4]}$$

$$-\Gamma q + 2\Delta D(1-s) = 0, \quad \text{[S5]}$$

indicating that graded input signals elicit polarization in an expectedly linear fashion. In the absence of nonlinearities, we recover that $q/s \approx \Delta D/D \ll 1$.

ii) $\alpha > 0$ and $\beta = 0$:

$$(1-s)(D-s)(2+\alpha s) - \Gamma s + \alpha q \Delta D(1-s) = 0 \quad \text{[S6]}$$

$$-\Gamma q + 2\Delta D(1-s) = 0. \quad \text{[S7]}$$

However, again, we recover that polarity is generated in linear response to graded inputs. The total concentration of heterodimers, s, on the other hand, is amplified by the positive feedback, the strength of which is quantified by α. Positive feedback alone cannot elicit spontaneous polarization. This is most clearly seen when we consider the heterodimer equations in the limit where the cellular stoichiometric constraints are disregarded. In this limit, $\beta = 0$, there are no interactions among heterodimers of opposing moieties.

iii) $\alpha = 0$ and $\beta > 0$: The steady-state relations for this set of interactions is

$$2(1-s)(D-s) - \Gamma s - \frac{1}{2}\Gamma\beta\left(s^2 - q^2\right) = 0 \quad \text{[S8]}$$

$$-\Gamma q + \Delta D(1-s)(2+\alpha s) = 0. \quad \text{[S9]}$$

In the limit of strong *cis* inhibition, $\beta \gg 1$, we recover that $s \approx q$ and $q \approx \frac{\Delta D(1-s)}{\gamma}$. This corresponds to the very "clean" limit where only the more abundant moiety of heterodimers is allowed to stabilize on an interface.

We outline an interesting twist on the above scenario supplementing heterodimer formation kinetics with the additional adaptation kinetics:

$$\frac{dz_{ij}}{dt} = \Gamma\beta U_{ij}U_{ji} - k^- z_{ij}. \quad \text{[S10]}$$

Here, z_{ij} is a complex that comprises two paired heterodimer complexes of opposite orientation, U_{ij} and U_{ji}. The strong *cis* inhibition limit, $\beta \gg 1$, ensures that every available pair of oppositely polarized heterodimers will form a new z-complex, symmetrical with respect to the interface it resides in. Although this model fails to explain the observations for reasons analogous to the pure $\alpha = 0$ and $\beta > 0$ model, it does stabilize two species of

complexes, U's and Z's, that respond to the mean and graded levels of an input signal, respectively.

iv) $\alpha > 0$ and $\beta > 0$:

$$(1-s)(D-s)(2+\alpha s) - \Gamma s - \frac{1}{2}\Gamma\beta\left(s^2-q^2\right) + \Delta D(1-s)\alpha q = 0 \quad \textbf{[S11]}$$

$$(1-s)(D-s)\alpha q - \Gamma q + \Delta D(1-s)(2+\alpha s) = 0. \quad \textbf{[S12]}$$

Setting $\Delta D = 0$, the bifurcation is described by the following condition:

$$q^2 = s^2 - \frac{4}{\alpha\beta} > 0, \quad \textbf{[S13]}$$

which clearly demonstrates that nonzero α and β are both required for spontaneous polarization. In the limit where $\Delta D = 0$, the dependence of s on D is

$$s = \frac{(D+1) \pm \sqrt{(D-1)^2 + \frac{4\Gamma}{\alpha}}}{2}. \quad \textbf{[S14]}$$

In the limit where $\Gamma/\alpha \ll 1$, we have $s \to D$ if $(D < 1)$ and $s \to 1$ (if $D > 1$). Naturally, the less abundant protocadherin limits the concentration of heterodimers that can stabilize at an interface. Were one to conduct the more elaborate analysis allowing Fat levels to vary as well, the above relation would relate s to Ω in the limit where $\Delta = 0$ (definitions are provided in the main text).

3. Instability Mode

The nature of the nonlinearities makes it clear that the instability is a long-wavelength one. That said, we present the calculation here for the sake of completeness.

We probe the linear stability by considering the dynamics of small perturbations about a symmetrical state:

$$U_1 = U_0 + A(t)e^{jki}; U_2 = U_0 + B(t)e^{jki}. \quad \textbf{[S15]}$$

Here, k is the wavenumber, i is the lattice index, and $j = \sqrt{-1}$.

Linearizing the governing equations gives

$$\frac{d}{dt}\begin{bmatrix} A \\ B \end{bmatrix} = M \begin{bmatrix} A \\ B \end{bmatrix},$$

where the matrix elements are

$$\begin{aligned}
M_{1,1} &= (1+\alpha U_0)(D+1-4U_0) + \Gamma\beta U_0 - \alpha(1-2U_0)(D-2U_0) + \Gamma \\
M_{1,2} &= \cos(k)(1+\alpha U_0)(D+1-4U_0) - j\,\sin(k)(1+\alpha U_0)(D-1) + \Gamma\beta U_0 \\
M_{2,1} &= \cos(k)(1+\alpha U_0)(D+1-4U_0) + j\,\sin(k)(1+\alpha U_0)(D-1) + \Gamma\beta U_0 \\
M_{2,2} &= (1+\alpha U_0)(D+1-4U_0) + \Gamma\beta U_0 - \alpha(1-2U_0)(D-2U_0) + \Gamma.
\end{aligned} \quad \textbf{[S16]}$$

We numerically solve the dispersion relation and sweep through D, the size of the uniform input signal. Fig. S1 shows that, indeed, the instability occurs at the theoretically predicted D^* and is a long-wavelength instability.

4. Polarization Response Is Level-Dependent

Here, we calculate the susceptibility, that is, the polarization response to a gradient at a given level. We probe the governing equations:

$$(1-s)(D-s)(2+\alpha s) - \Gamma s - \frac{1}{2}\Gamma\beta\left(s^2-q^2\right) + \Delta D(1-s)\alpha q = 0 \quad \textbf{[S17]}$$

$$(1-s)(D-s)\alpha q - \Gamma q + \Delta D(1-s)(2+\alpha s) = 0, \quad \textbf{[S18]}$$

with the ansatz

$$s = s_0 + s_1 + \mathcal{O}\left(\Delta D^2\right); q = q_0 + q_1 + \mathcal{O}\left(\Delta D^2\right), \quad \textbf{[S19]}$$

resulting in

$$q_1 = \Delta D \frac{s_0(1-s_0)(2+\alpha s_0)}{\alpha q_0^2 \sqrt{\left(d^0 - f^0\right)^2 + \frac{4\Gamma}{\alpha}}}. \quad \textbf{[S20]}$$

The various terms in the susceptibility are intuitive: (*i*) No additional polarization is achieved when there are either no or saturated concentrations of heterodimers, $s_0 = 0$ and $s_0 = 1$, respectively; (*ii*) tuning to the onset of spontaneous polarization leads to a diverging susceptibility and correlation length, $1/q_0^2$; and (*iii*) a second peak in the susceptibility is observed when $d^0 \approx f^0$, which diverges in the limit $\Gamma \to 0$ or $\alpha \to \infty$. This, of course, corresponds to extreme depletion effects mediated by stoichiometric competition.

To confirm this second peak, we conduct a perturbation analysis around a nonlinear base state:

$$U_{i,i+1} = U_+ + A(t)e^{jki}; U_{i+1,i} = U_- + B(t)e^{jki}, \quad \textbf{[S21]}$$

giving

$$\begin{bmatrix} \dot{A} \\ \dot{B} \end{bmatrix} = N \begin{bmatrix} A \\ B \end{bmatrix},$$

where the matrix elements are

$$\begin{aligned}
N_{1,1} &= (1+\alpha U_-)(D+1-2s) + \Gamma\beta U_+ \\
N_{1,2} &= \cos(k)(1+\alpha U_-)(D+1-2s) - j\,\sin(k)(1+\alpha U_-)(D-1) + \Gamma\beta U_- \\
N_{2,1} &= \cos(k)(1+\alpha U_+)(D+1-2s) + j\,\sin(k)(1+\alpha U_+)(D-1) + \Gamma\beta U_+ \\
N_{2,2} &= (1+\alpha U_+)(D+1-2s) + \Gamma\beta U_-.
\end{aligned} \quad \textbf{[S22]}$$

We explore the dispersion relation numerical as we did for the symmetrical state previously. Because the instability is long-wavelength and generically parabolic near $k = 0$, we approximate $\sigma = \sigma_0 - \sigma_2 k^2$ and define the correlation length to be $\ell \sim \sqrt{\frac{\sigma_2}{\sigma_0}}$. Fig. S2 highlights the characteristic features of the correlation length and its dependence on protocadherin levels. We, of course, recover the divergence in the correlation length at the critical point itself and at a second peak at $D = 1$, corresponding to the scenario where the protocadherins are equally abundant.

5. Iso-Signaling Contours

The expression for susceptibility also gives us the shape of protocadherin profiles along which polarization is constant. Taking the limit where $d^0 > f^0$ in the susceptibility

$$q_1 = \Delta D \frac{s_0(1-s_0)(2+\alpha s_0)}{\alpha q_0^2 \sqrt{\left(d^0 - f^0\right)^2 + \frac{4\Gamma}{\alpha}}} \quad \textbf{[S23]}$$

results in

$$q_1 \sim \frac{\Delta D}{D}, \qquad \text{[S24]}$$

agreeing with the visual observation of contours as approximately straight lines emanating from the apex of the signaling wedge at $d^0 = f^0$ in the signal transduction map. Naturally, different values of q_1 pick out different contours on the signal transduction map corresponding to different levels of uniform pathway activity. Any one contour is therefore described by one parameter, λ^{-1}, the ratio of graded to level input signal, which suggests that approximately exponential profiles (that preserve the ratio of gradient to level) generate uniform pathway activity. The fact that $q_0 \neq 0$ imposes that the exponential profiles must asymptote to a constant rather than zero. The details of the relationship between λ and y, nuclear Yorkie levels, depend on details of the model for the Hippo pathway, but, broadly, it follows a relationship as depicted in Fig. S3*B*.

6. General Considerations of Noise Reduction

In general, if the mean number of molecules of a species is N, we expect $\sqrt{N}$ to be the order of fluctuations. Because the number of molecules in each cell may be small, these stochastic fluctuations may deteriorate the fidelity of signaling. In particular, the levels of morphogen, total Fat and Ds, and U_{0ij}s may be considerably noisy. Two factors are of importance in reducing the effect of noise in the signal transduction pathway: (*i*) temporal averaging of signal transduction fluctuations that occur on the time scale much faster than the characteristic time of cell growth and division and (*ii*) spatial averaging due to cell–cell signaling.

Time Scales. There are many intermediate signal transduction steps between morphogen gradients and cellular growth, and, in fact, some of these steps may be quite noisy. For example, the polarization at an interface may have increased stochasticity due to positive feedback, particularly near the bifurcation point. The effect of noise on the fidelity of signaling is limited by the fact that cellular growth is much slower than the signaling processes. Roughly speaking, a slow-growing cell measures the instantaneous level of intermediate signaling species multiple times, $\tau_\gamma / max\{\tau_D, \tau_t, \tau_K\}$, thereby reducing (averaging) the noise by the square root of this ratio.

Spatial Averaging. A natural consequence of cell–cell interactions is correlations between the signaling species of neighboring cells. Therefore, any noise in the morphogen level is averaged over a patch of correlated cells. The correlation length, ξ (in units of cells), determines the scale over which the signal is averaged. The variance and mean are both averaged similarly; hence, the effective signal to noise improves by $\sqrt{\xi}$.

7. Four-Jointed

Here, we present a simple extension to our model that accounts for Four-jointed (Fj). There is evidence that Fj increases the affinity Fat has for Ds and decreases the affinity Ds has for Fat. This double (and opposing) effect indicates that one cannot interpret Fj as modulating k_u in the kinetics of heterodimer formation, because an increase in this rate constant would ensure an increase in Fat to Ds and Ds to Fat binding:

$$\frac{dU_{ij}}{dt} = k_u f_i d_j \left(1 + \alpha U_{ij}^m\right) - \gamma_u U_{ij} \left(1 + \beta U_{ji}^{m'}\right). \qquad \text{[S25]}$$

An alternative is to posit that Fj alters the pool of Fat in a cell that is available to bind to Ds in adjacent cells. Mathematically,

$$f_i^0(Fj_i) = f_i + \sum_{\{j\}_i} U_{ij} \;\; and \;\; d_i^0 = d_i + \sum_{\{j\}_i} U_{ji}, \qquad \text{[S26]}$$

where the f_i^0 increases with the level of Fj in cell i. Opposing Ds and Fj transcriptional profiles can therefore be interpreted as opposing profiles in "ready-to-bind" protocadherin, Ds, and Fat. Although this interpretation of the role of Fj is simplistic, it reflects our lack of knowledge as to how Fj modulates differential affinity.

Fat pathway activity alters Fj expression in a cell, suggestive of feedback within the Fat pathway. Constraining models for such feedback would require live imaging of Fat pathway activity and Fat pathway components.

8. Dachs Inhibition

Eq. **3** is reproduced below:

$$c_{ij} = \frac{\sigma}{1 + \left(U_{ij}/\overline{U}\right)^{m_c}}. \qquad \text{[S27]}$$

We now describe how this steady-state relationship between membrane-accumulated Dachs and active Fat is arrived at. Note that an alternative model for Dachs could be the partitioning of a cellular pool of Dachs to cellular membranes, but this is not what we do here. There is a pool of Dachs associated with each membrane that is inhibited by active Fat on that membrane. We will return to a discussion of this once we have considered this much more local model:

$$\frac{dc_{ij}}{dt} = k_c^+ - k_c^- c_{ij} - k_{c,u}^- c_{ij} U_{ij}^{m_c}. \qquad \text{[S28]}$$

The above equation is straightforward. Ignoring the last term (with the U_{ij}), the rate of change of Dachs at a membrane is due to Dachs arriving at the membrane at a rate k_c^+ and the degradation of Dachs at a rate k_c^-. This itself will set a steady-state level of Dachs (steady state is defined to be the concentration at which the rate of change in time is zero, mathematically, $\frac{dc_{ij}}{dt} = 0$, at some c_{ij}^{s-s}) that is $c_{ij}^{s-s} = k_c^+/k_c^-$, the ratio of the two kinetic rates. We can now ask how the additional inhibition of Dachs by active Fat alters the steady-state level calculated here. Searching out the steady-state Dachs concentration with active Fat inhibition, we arrive at

$$c_{ij}^{s-s} = \frac{k_c^+}{k_c^- + k_{c,u}^- U_{ij}^{m_c}}. \qquad \text{[S29]}$$

Eq. **3** is this steady state upon identifying $\sigma = k_c^+/k_c^-$ and $\overline{U} = (k_c^-/k_{c,u}^-)^{1/m_c}$. Note that we have allowed the inhibition of Dachs by active Fat to be nonlinear, represented mathematically by m_c. Although we allow for this, we do not use this in our analysis and stick to a simple linear inhibition of Dachs by active Fat, that is, $m_c = 1$.

We now consider an alternative model where there is a fixed pool of cellular Dachs that diffuses along the membrane. This stands in contrast to the above model, where the membrane has its own pool of Dachs that either localizes to it or is inhibited by the active Fat population at that membrane. The level of active Fat along all cell membranes would inhibit the cellular pool of Dachs (i.e., it would determine the level of Dachs; one can imagine the above kinetic equation instead of being membrane by membrane for the whole cell). The concentration of Dachs that is not inhibited would now be free to diffuse along cell membranes, ensuring that Dachs polarity would be lost. Hence, such an inhibition diffusion model for Dachs would not recover Dachs polarity. To recover polarity within a diffusion model, we would have to introduce local "sinks," with those being local active Fat providing local inhibition of Dachs. This is our justification for considering the local mode of Dachs inhibition presented in our paper.

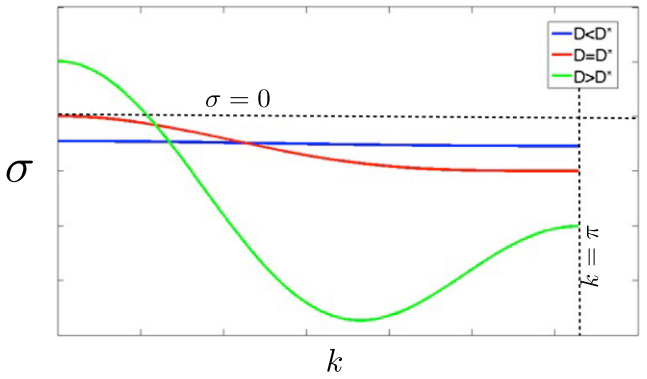

Fig. S1. Numerical evaluation of dispersion relation. The eigenvalue, σ, is plotted as a function of the mode, k, and for three different values of D, the uniform input signal. It is observed that at criticality, $D = D^*$, an eigenvalue becomes positive, thereby admitting a growing mode. The fastest growing mode is a long-wavelength one, $k = 0$.

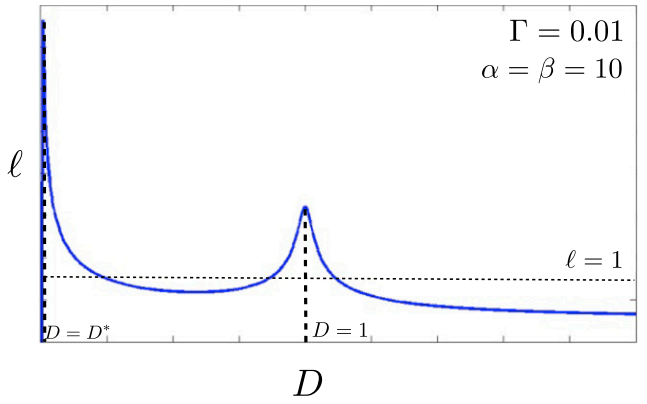

Fig. S2. Numerical calculation of the correlation length. Because the dispersion relation has a parabolic shape close to $k = 0$, described by $\sigma = \sigma_0 - \sigma_2 k^2$, we estimate the correlation length to be $\ell \sim \sqrt{\frac{\sigma_2}{\sigma_0}}$. The divergence at the critical point and the second peak when Fat = Ds is reproduced, agreeing with the susceptibility calculation (here, D is the level of Ds relative to Fat).

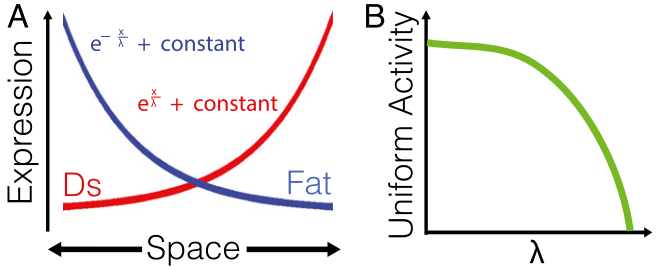

Fig. S3. Iso-signaling/growth protocadherin profiles. (*A*) Shifted exponential profiles of protocadherins, corresponding to contours of Fig. 3*A*, generate uniform pathway activity in the model. (*B*) Steepness of protocadherin profiles, λ^{-1}, determines the degree of uniform Fat pathway activity. Shallow profiles correspond to lower pathway activity.

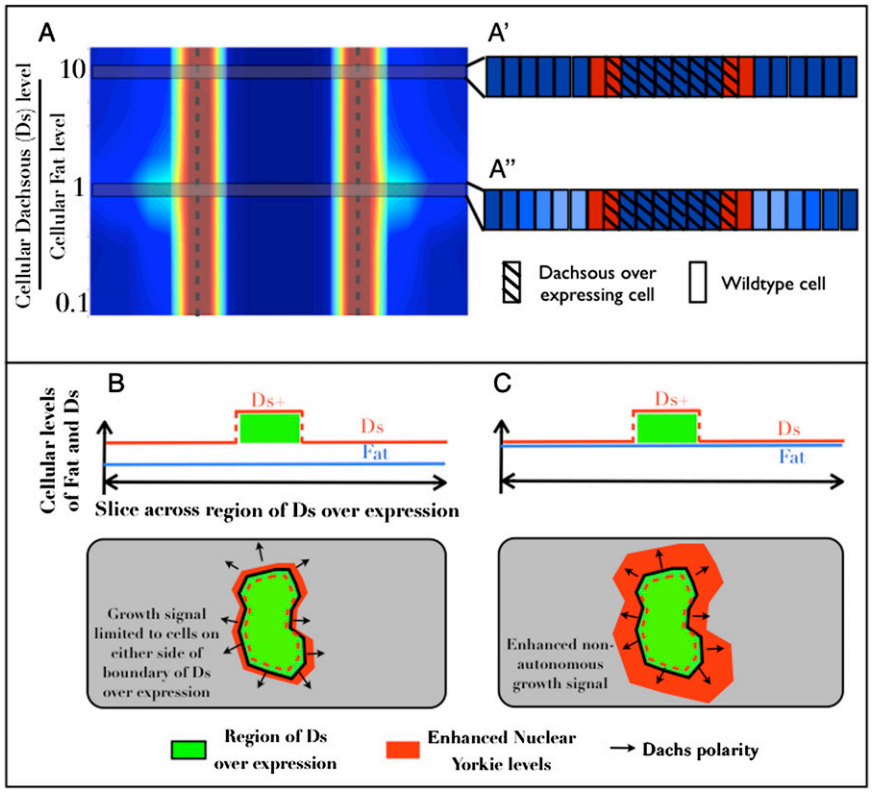

Fig. S4. Variation in nonautonomous response. (*A*) Horizontal slices (*A′* and *A′′*), numerical simulations of the model, correspond to a line of cells where Ds is locally overexpressed. Different horizontal slices correspond to different relative (to Fat) Ds levels in the surrounding cells. The degree of nonautonomous induction of growth is maximal when Ds and Fat are equally abundant. (*B* and *C*) Illustrations of the predicted responses.